

Robust Fluorescent Response of Micropatterned Multilayered Films

SRIKANTH SINGAMANENI,¹ CHAOYANG JIANG,¹
EMILY MERRICK,² DINESH KOMMIREDDY,³
AND VLADIMIR V. TSUKRUK¹

¹Department of Materials Science and Engineering, Iowa State University, Ames, IA and School of Materials Science and Engineering, Georgia Institute of Technology, Atlanta, GA

²Department of Materials Science and Engineering, Iowa State University, Ames, IA

³Institute for Micromanufacturing, Louisiana Tech University, Ruston, LA

We demonstrate that photobleaching can be significantly suppressed in fluorescent-labeled polyelectrolyte layer-by-layer (LbL) films by efficient spatial isolation of the dye molecules using multilayered architecture. The films exhibited excellent temporal stability under high excitation power where the bulk films suffered a significant photobleaching. Quenching of the fluorescence caused by the resonant energy transfer between the dye molecules and gold nanoparticles exhibited a weak distance dependence with significant quenching extending beyond 20 nm distance. The robust, freely suspended, fluorescent LbL films exhibited stable fluorescence response under deformation which can make them attractive for sensitive fluoroimmunoassays.

Keywords atomic force microscopy, energy transfer, fluorescence, LbL films, photobleaching

Introduction

Fluoroimmunoassay detection based on controlled energy transfer has been very successful over the last decade due to the relative ease in read-out process and unique optical signature.^[1,2] Such techniques have been applied for the detection of DNA,^[3,4] proteins,^[5] and specific antigens.^[6,7] The same phenomenon is also employed to monitor biological processes such as protein folding^[8] and conformational changes.^[9] Quenching of fluorescence of dye molecules adsorbed on the surface of metal due to non-radiative energy transfer mechanism is one of the key techniques for biological detection.^[10] Particularly, Förster resonant energy transfer^[11] (FRET) between

Received 2 June 2006; Accepted 6 July 2006.

In Commemoration of the Contributions of Professor Valery P. Privalko to Polymer Science.

Address correspondence to Vladimir V. Tsukruk, School of Materials Science and Engineering, Georgia Institute of Technology, Atlanta, GA 30318, Fax: 404-894-9140. E-mail: vladimir@mse.gatech.edu

the excited dye molecule acting as donor and the acceptor species is exploited for the non-radiative energy transfer and controlled quenching of the fluorescence of the dye molecules. Compared to organic acceptor molecules, gold nanoparticles have been proven to be much stronger quenchers of molecular excitation of fluorophore. However, the quenching of the fluorescence of the chromophore near the surface of a metal nanoparticle is not only due to energy transfer between the chromophore and the metal nanoparticle but is also caused by alternation in the radiative and non-radiative rates of the chromophore's de-excitation process.^[12,13] The energy transfer rates, which are one of the primary factors of the quenching mechanism, depend significantly on the size and shape of the nanoparticles and distance between the dye molecule and the metal nanoparticle.^[10,14]

Photobleaching is one of the most important issues in applications involving low concentration fluoroimmunoassay techniques and single molecule fluorescence spectroscopy. Photobleaching is an irreversible photochemical process making a fluorophore permanently lose the ability to fluoresce.^[15] It is a complex photochemical process, involving dye-dye and dye-ambient interactions. In the studies involving the tracking of a biological process over extended time, photobleaching can make it impossible to complete the experiment. On the other hand, fluorescence recovery after photobleaching (FRAP) can be used to study the dynamics of diffusion of various species.^[16,17]

Several chemical and physical approaches have been suggested to minimize the photobleaching effect, such as adding antifading agents^[18] and increasing the laser intensity at the same rate as the photobleaching to compensate for the lost fluorescence.^[19] All these methods rely on either an additional constituent in the fluorescent system or on a tedious procedure to establish the experimental routine to overcome the photobleaching problem. The fluorescence behavior of the molecules in solution is known to be significantly different from that in the solid state.^[20] This is related to a high degree of interaction between the closely packed molecules in the solid causing intermolecular energy transfer. This interaction leads to several different effects such as homo-resonance energy transfer (RET),^[21] shifts in the absorption and emission spectra,^[22] and photobleaching. A solid state system with isolated molecules, resembling the solution state, could minimize the unwanted effects (homo RET and photobleaching) inherent in a conventional bulk counterpart.

In this communication, we report a novel method for the partial suppression of the photobleaching effect in ultrathin films by separating fluorescent labels confined within a nanoscale layer (about 1.5 nm thick) with another nanoscale (1.5 nm) neutral polymeric layer (bilayer structures), thus significantly reducing non-radiative energy transfer due to dye-dye interactions. We investigate the resonant energy transfer mechanism in such multilayered structures with a controlled number of bilayers by using micropatterned gold nanoparticle arrays. The quenching efficiency of gold nanoparticles on differently positioned bilayer (dye/non-dye) structures was studied as a function of the number of bilayers and less dramatic distance dependence than that predicted by the theory for uniform medium was observed. The stability of the fluorescent response against mechanical perturbations was demonstrated by deforming the freely suspended fluorescent nanomembrane under hydrostatic pressure.

Layer-by-layer (LbL) assembly, which provides a precise control over the position of the components along the thickness of the structure, was chosen to build such a system because of its unique ability to control the placement of different species in a regular manner.^[23,24] Thus, we employed LbL assembly which involves the alternate adsorption of oppositely charged polyelectrolytes for the fabrication of ultra thin polymer films with precise control over geometry down to a single nanometer.^[25–28] The multilayered

polyelectrolyte films can be highly robust and exhibit exceptional mechanical stability, optical activity, bio-compatibility, and electrical conductivity.^[29–34]

Experimental

Poly (sodium 4-styrenesulfonate) (PSS) was purchased from Aldrich and used without further purification. Poly (allylamine hydrochloride) (PAH) was purchased from Aldrich and labeled with rhodamine B isothiocyanate (RITC) (1% labeling) according to the known procedure.^[35] In brief, PAH solution (60 mg/ml) in 0.1 M NaHCO₃ was added to RITC in DMF (0.25 g/ml) and stirred for 1 h at room temperature. Subsequently, RITC-PAH conjugate, called PAH* hereafter, was precipitated and re-suspended in Tris buffer. Chemical structure of the PAH* is shown in Fig. 1a and the RITC/PAH ratio was 1/100. Gold nanoparticles of diameter 13 nm were synthesized by the reduction of tetrachloroauric acid using sodium citrate.^[36] The UV-vis absorption of the PAH* solution and the gold nanoparticle solution was obtained using a Shimadzu UV 1601 spectrophotometer.

Multilayer films of oppositely charged polyelectrolytes with a structure of (PAH*/PSS)_n, were fabricated using spin assisted LbL in a class 100 clean room as reported in detail elsewhere.^[37,38] LbL films with a surface-patterned gold nanoparticle array, (PAH*/PSS)_n PAH*/Au, designated as n*G, where n (1 to 9) is the number of bilayers,

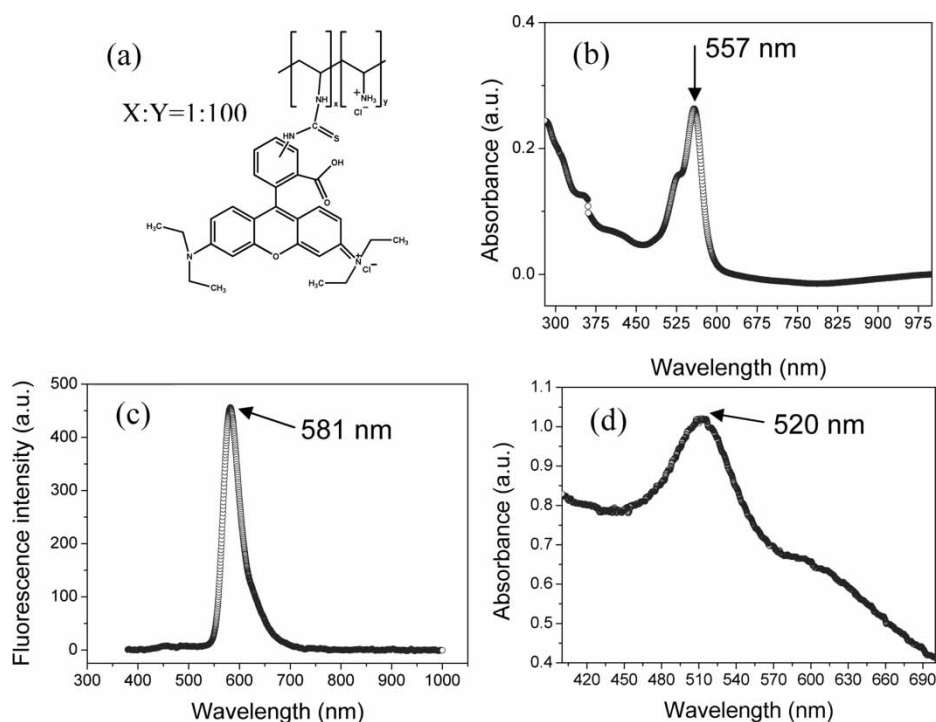


Figure 1. (a) Chemical structure of fluorescent labeled (Rhodamine B isothiocyanate) PAH*. (b) UV-vis absorption spectra of bulk PAH*. (c) Fluorescence emission spectra of PAH* solution under an excitation of 365 nm. (d) UV-vis of gold nanoparticles solution showing the surface plasmon absorption.

were fabricated for FRET experiments according to the known procedure.^[34] In the case of the free standing films, additional polyelectrolyte multilayers were deposited on the gold nanoparticles completely encapsulating them in the membranes making the resulting structure to be n^*Gn^* . Water from a Nanopure system (18 M Ω cm) was used for preparation. The cast sample was prepared by drop casting the PAH* solution (0.2% v/v) on a glass slide and drying the sample under vacuum (10^{-3} Torr) for 24 h.

The morphology of the LbL films was studied with a Dimension 3000 Atomic Force Microscope (AFM) according to the procedure adapted in our lab.^[39,40] The micropatterned array of gold nanoparticles on the LbL films was inspected with an optical microscope (DM 4000M, Leica) in reflection mode. Fluorescence spectra and images of the membranes with gold nanoparticles were obtained with the DM 4000M microscope equipped with a Craic single-spot fluorescence spectrometer. Time-dependent fluorescence was studied using a custom-designed confocal Raman-fluorescence instrument based on an Aurora-III near-field scanning optical microscope with a Nd:YAG laser (532 nm wavelength) as the excitation source as described elsewhere.^[41]

Results and Discussion

Fluorescence of bulk and LbL films. The absorption maxima of the PAH* solution was found to be at 557 nm (see UV absorption spectra in Fig. 1b). The fluorescence spectra of PAH* solution obtained with an excitation wavelength of 365 nm displays a strong peak at 581 nm (Fig. 1c). These spectra completely agree with the data reported in the literature.^[42] Finally, the plasmon absorption with a peak at 520 nm was observed for the solution of 13 nm gold nanoparticles used in the FRET experiments (Fig. 1d). It is worth mentioning that there is a significant overlap between the fluorescence emission of the PAH* and gold nanoparticle plasmon adsorption, which is one of the primary requirements for the efficient energy transfer for the donor-acceptor pair.^[14]

The microlayered structure of LbL films designed here includes PAH* layers with the fluorescent labels separated by interlacing PSS layers (Fig. 2a). The thickness of the LbL assembled films, as determined from topographical cross-sections of AFM scanning along the edge of the film, increased linearly with the number of bilayers with an increment of 3.1 nm for each bilayer, thus giving a thickness of a single layer of about 1.5 nm. All

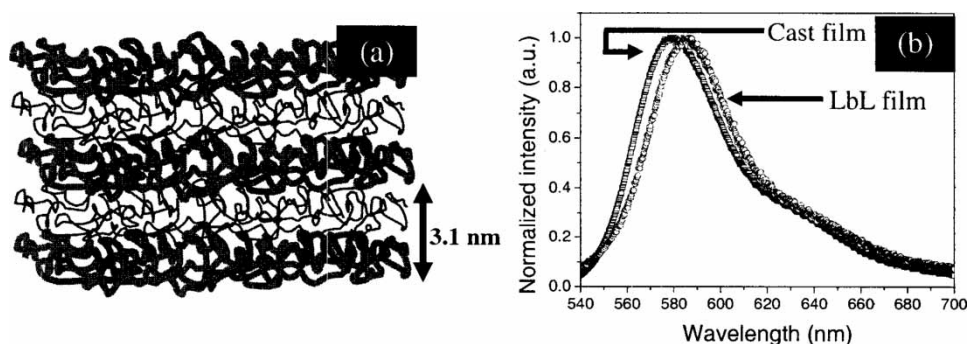


Figure 2. (a) Schematic representation of the LbL structure of alternating PAH* and PSS layers. (b) Fluorescence spectra of cast PAH* film and 9-bilayer LbL film depicting the blue shift in the cast film.

values are fairly close to that well-known in the literature.^[26] The 9-bilayer LbL film which was used as a representative sample in the photobleaching experiments had a thickness of 28 nm and a smooth surface with microroughness for the surface area of $1 \times 1 \mu\text{m}^2$ below 1.7 nm.

Fig. 2b shows the fluorescence spectra of the cast PAH* film (thickness about 3 μm) and (PAH*PSS)₉ LbL film. A small red-shift in the fluorescence peak was observed if PAH* layers were separated by PSS layers. The peak position for the LbL film closely matched (difference of less than 1.5 nm) that in the solution. The 7 nm blue shift for bulk PAH* film can be attributed to the aggregation of the dye molecules resulting in increased interaction between them.^[43] It is known that H-aggregates exhibit a blue shift while J-aggregation results in red shift of the emission spectra.^[44] The blue shift of the H-aggregates is due to the exciton splitting where the lower energy level is optically forbidden and the transition can only occur from the upper level to the ground state.^[22]

Photobleaching in bulk and LbL films. Temporal decay of the fluorescent intensity due to the photobleaching of the fluorophores under laser excitation was studied for cast PAH* films and multilayered LbL films. Fig. 3a shows the time resolved (collected with 1s

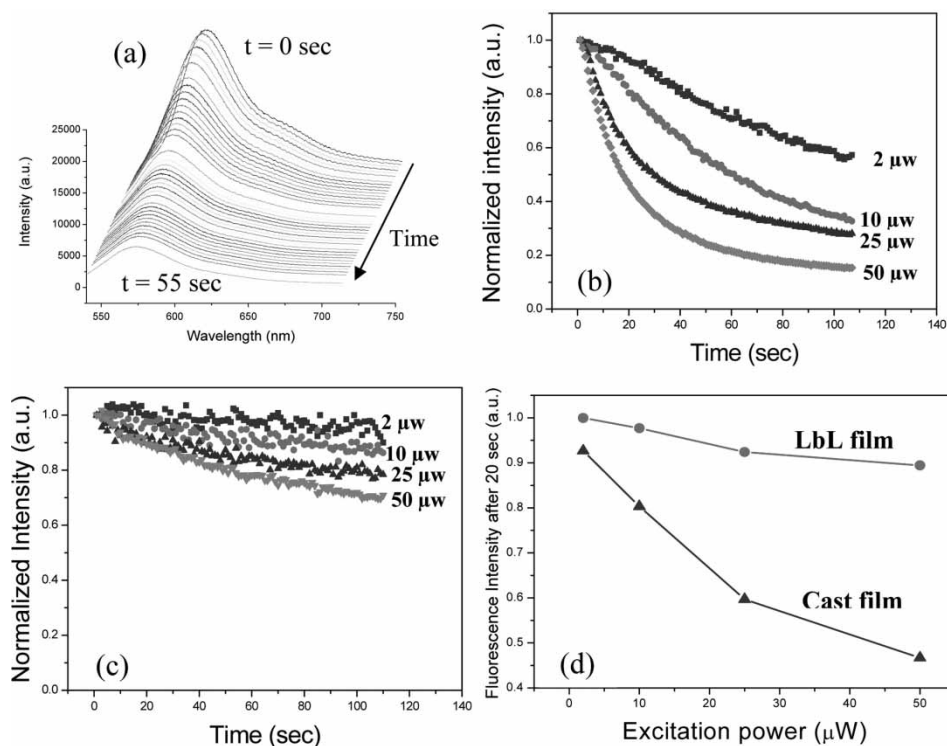


Figure 3. (a) Time resolved fluorescence spectra (excitation power $4 \times 10^4 \text{ W/cm}^2$) of the cast PAH* film depicting the decaying intensity due to photobleaching. (b) Photobleaching phenomenon for cast PAH* film for various powers of the excitation source. (c) Photobleaching phenomenon for 9-bilayer LbL films for various powers of the excitation source. (d) Fluorescence intensity retained vs. the excitation power after 20 s for cast and LbL films.

interval) fluorescence spectra of the cast film with an excitation power of 50 μW over a 400 nm diameter area ($4 \times 10^4 \text{ W/cm}^2$ power). It is worth noting that the initial intensity of the fluorescent peak for cast PAH* film was nearly eight times higher than that for LBL film if obtained under identical experimental conditions. This difference is caused by the larger thickness of the cast film and different composition (e.g., PSS presence in the LbL film).

The normalized fluorescence intensity of the cast film and the LBL film as a function of time for various laser powers is shown Figs. 3b and 3c, respectively. Apparently, in both cases the rate of photobleaching increases with the increasing laser power. However, the photobleaching in the case of the LbL films is much smaller as compared to that of the cast films. Fig. 3d shows that the fluorescence intensity retained after 20 s for different laser powers is much higher for the LbL films. For instance, for 50 μW power the cast bulk film suffers from a rapid photobleaching with an intensity decay of 90% in the first 120 s. On the other hand, under the same illumination intensity the LBL film shows a decay of less than 25%. For 50 μW laser intensity the LBL films exhibit nearly 40% higher fluorescence intensity retention compared to the cast film indicating much higher photobleaching stability of the LbL films as compared to bulk PAH* material.

Such a difference can be understood considering that several concurrent processes can contribute to the photobleaching phenomenon which include dye-dye (D-D), dye-oxygen (D-O), and dye-photon (D-P) interactions.^[15,45] One of the important processes of the non-radiative energy transfer mechanism is where the electron in the excited singlet state transfers to the excited triplet state and returns to the ground state in a non-radiative manner. This process can occur due to the resonant intermediate states of the oxygen from the ambient and the neighboring dye molecules. In the bulk film the state crossing is promoted by the aggregation of the fluorescent molecules. However, in the LbL multi-layered structures the fluorescent molecules are separated by 1.5 nm thick PSS layers, thereby decreasing the possible interactions across layers (Fig. 2a). Thus, the layered LbL architecture partially suppresses the cross-talks in the vertical direction. One should note that such non-radiative mechanism might still persist to some extent in LbL films due to the proximity (average separation of 15 nm estimated from the labeling percentage) of the molecules within the same layer.

RET between labeled layers and gold nanoparticles. Quenching of fluorescence due to RET between the excited dye molecule and a proximal metal surface is one of the most common sensing mechanisms in fluoroimmunoassays. To investigate the quenching behavior of these multilayered structures, we designed micropatterned LbL films with selectively placed gold nanoparticles (Fig. 4a). In this design, the PAH* layer closer to the gold nanoparticles is highly sensitive to the RET but controlled distance of separation occurs for increasing number of bilayers. On the other hand, the micropatterned samples offer the unique advantage of obtaining the fluorescence signal simultaneously from the areas with and without gold nanoparticles making the quantitative comparison unambiguous.

The optical image of Fig. 4b shows the 9*G film with a uniform pattern of gold nanoparticles deposited on the LbL film surface and extending over large distances. The brighter stripes on the image correspond to a monolayer of gold nanoparticles with higher reflectivity as was proved by cross-sectional analysis as discussed in our previous publication.^[37] The micropatterned morphology is confirmed with AFM (Fig. 4c). The elevated stripes from LbL films with encapsulated gold nanoparticles are

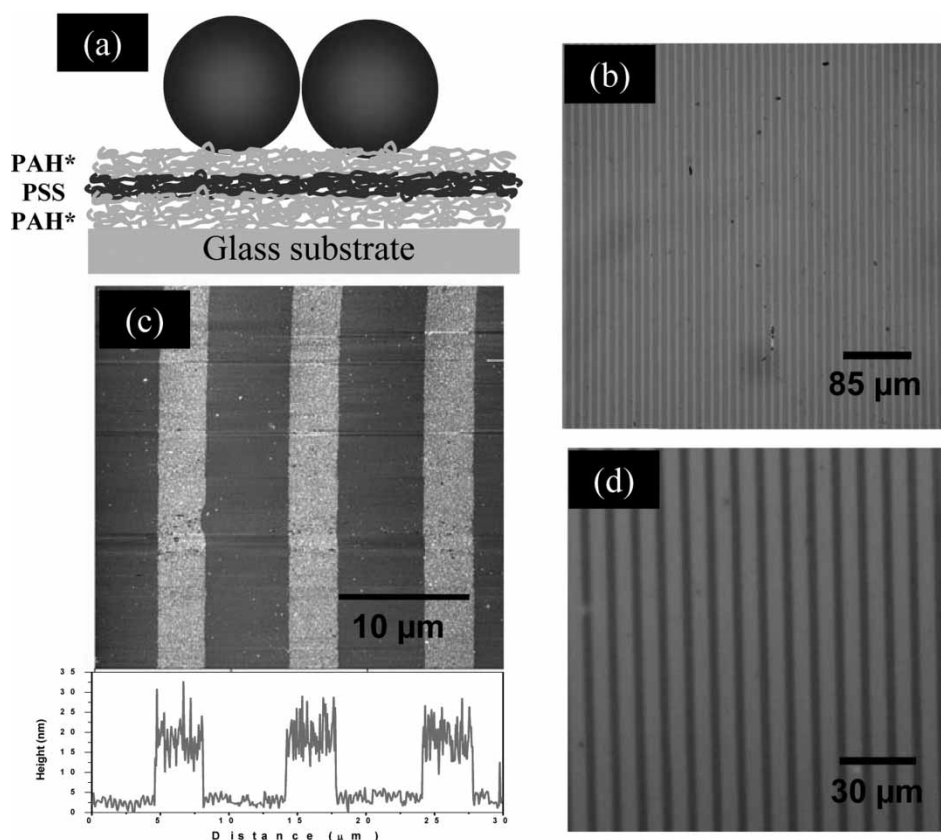


Figure 4. (a) Schematic representation of the LbL film with gold nanoparticles on the surface of the film. (b) Optical micrograph of the 9*G film showing uniform micropattern over large surface area. (c) AFM image depicting the high selectivity of the micropatterned gold nanoparticles and the corresponding cross-sectional height profile showing the alternating regions with and without gold nanoparticles. (d) Fluorescence image of the 9*G film with the dark and bright areas representing the areas with and without gold nanoparticles, respectively.

3 micron wide and 43 nm thick. This is 13 nm thicker than that of the area without gold nanoparticles, indicating a monolayer of gold nanoparticles with diameter close to 13 nm. The gold nanoparticle with modest negative charge under normal pH conditions were stable in solution state and readily adsorbed on the positively charged PAH terminated surface making relatively densely packed monolayers. In the final assembly, alternating layers of negatively charged nanoparticles and positively charged polyelectrolytes made LbL films very stable due to strong Coulombic interactions. Fig. 4d shows the fluorescence image of the LbL film with the dark stripes of the image representing low fluorescent intensity areas corresponding to the gold nanoparticle areas and the brighter areas corresponding to the surface areas without gold nanoparticles. The presence of gold nanoparticles efficiently quenches the fluorescence of the PAH resulting in a pronounced contrast in the intensity, with the reversed contrast if compared with the optical image. The fluorescence spectral mapping obtained from the areas with and without gold nanoparticles for LbL films shows a clearly defined micropattern as well

(Fig. 5a). Fluorescence spectra from the film areas with and without gold nanoparticles differ significantly in the intensity of their main peaks with overall intensity changing periodically as can be seen from corresponding cross-section (Fig. 5b).

Figs. 6a and 6b show the fluorescence spectra of the LbL films with different numbers of bilayers. Significant increase in the fluorescence intensity with the increasing numbers of bilayers is observed as expected for LbL film with a linear growth mode. Similarly, the fluorescence intensity increases with increasing film thickness for LbL areas covered with gold nanoparticles, their overall intensity remaining much (three times) lower (Fig. 6b). Fig. 6c shows the linear variations of the fluorescence peak intensity with the number of bilayers for LbL films with and without gold nanoparticles on top. Apparently, the fluorescence intensity grows linearly in both cases with the overall intensity for LbL films covered with gold nanoparticles staying well below that for the rest of the LbL film due to significant quenching caused by the presence of the gold nanoparticles on top of growing LbL films (Fig. 4a). However, the overall slope of the intensity variation vs. the number of bilayers is different for the surface areas covered or not covered by gold nanoparticles.

For quantitative characterization of the quenching phenomenon, we calculated the fluorescence quenching efficiency η as

$$\eta = 100 \left(1 - \left(\frac{I_G}{I_{NG}} \right) \right) \quad (1)$$

where I_G is the intensity in the film areas covered by gold nanoparticles, I_{NG} is the intensity in the surface areas of the purely polymeric LbL film. The value of the η quantifies the percentage of the fluorescence intensity lost due to the non-radiative energy transfer between the membrane and the gold nanoparticles. The quenching efficiency of the gold nanoparticle for nanomembranes with different number of bilayers is shown in Fig. 6d. Apparently, for the first five bilayers (within 15 nm distance from gold nanoparticles), the quenching efficiency rapidly decreases by 40% followed by a very low rate of decay for higher number of bilayers. It is worth noting that the quenching efficiency remains constant for different laser powers.

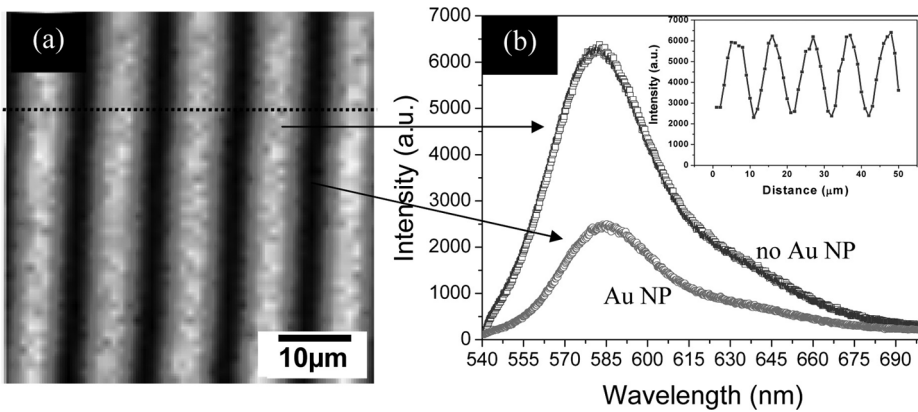


Figure 5. (a) Confocal fluorescence mapping of 6*G film under 532 nm excitation. (b) Fluorescence spectra of the 6*G film from selected areas (400×400 nm) with and without gold nanoparticles. Inset shows the variation of fluorescence intensity profile of the dotted line shown in the fluorescence map.

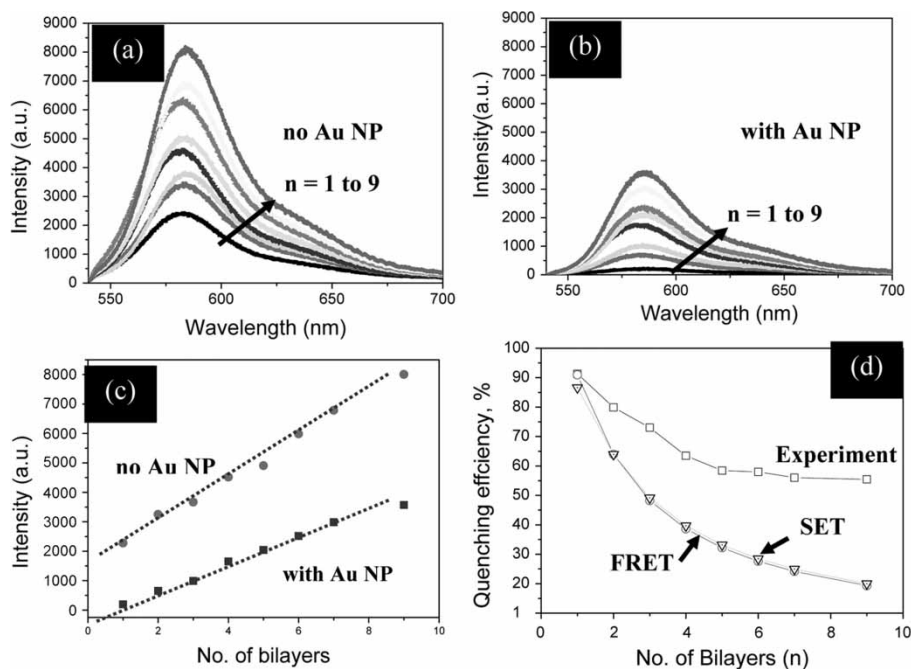


Figure 6. Fluorescence spectra of the LbL films with different of bilayers from the surface areas without (a) and with (b) gold nanoparticles. (c) The corresponding peak intensity vs. the number of bilayers. (d) The quenching efficiency vs. the number of bilayers from the experiment and calculated from theories.

Although the overall decrease of the quenching efficiency with the increasing distance is expected, its relatively high value (55%) even for larger distances is puzzling. As is known, the distance decay of the quenching efficiency is highly sensitive to the distance only in close proximity (2–10 nm) to the metal surfaces with quenching virtually disappearing for distance higher than 10 nm.^[46] According to the FRET theory, the energy transfer efficiency near a metal nanoparticle scales to the inverse sixth power of the distance if the nanoparticle is assumed to be a single dipole.^[11,47] However, in our case, a single dipole approximation is not valid due to dimension factors (nanoparticle diameter 13 nm in comparison with bilayer thickness 3.1 nm). Thus, if the nanoparticle is approximated as a dipole array (surface energy transfer (SET) theory), the distance dependence of the energy transfer efficiency should decrease as inverse fourth power.^[10,48,49]

$$E = \frac{1}{1 + (R/R_0)^4} \quad (2)$$

where R_0 is the characteristic distance at which the non-radiative energy transfer efficiency equals the radiative decay and R is the distance of separation between the gold nanoparticle and the fluorophore.

Theoretical quenching efficiency η_i for LbL films with i bilayers can be computed as $\eta_i = \sum_{j=0}^i \eta_j / i + 1$ where η_j is the quenching factor of PAH* layer separated by $(j - 1)$ bilayers from the quenching surface. The theoretical estimations of the quenching factor in accordance with the FRET and SET theories show a fast decay with the number of

bilayers (distance from the quenching surface) with a 80% reduction of the quenching efficiency predicted for 28 nm thick LbL films (Fig. 6d).

However, the experimentally observed quenching efficiency remains much higher (close to 55%) for the larger number of bilayers than that predicted by theoretical estimation. This high quenching efficiency can be associated with such important factors as orientation distribution of the chromophore groups confined within the PAH* monolayer with 1.5 nm thickness which can lead to additional coupling with the gold nanoparticles and affect the radiative or non-radiative transfer rates. It has been previously suggested that if the excitation of the donor is delocalized over large distances, the distance dependence of the non-radiative energy transfer is significantly weaker reaching quadratic dependence.^[50] Even more recently, it has been shown that a high quenching efficiency (45%) exists even when the fluorescent dye and the metal nanoparticles are separated by a distance of 8 nm.^[51] In their study the nanoparticles and the dye molecules were separated by polyelectrolyte bilayers. In our study, the presence of fluorescent monolayers spaced from the metal nanoparticles with bilayers makes it an interesting system in terms of a competitive non-radiative energy transfer between the gold surface and bilayers close to the nanoparticles and those located at the increasing distance.

Our results show that although fast reduction of the quenching occurred over the initial few bilayers (~ 10 nm distance), the quenching efficiency remains very high (several times higher than that predicted by theory) for larger distance. Although this phenomenon requires additional investigation, here we can speculate that our peculiar microlayered structure with alternating oppositely charged ionic species offers an efficient pathway for the energy transfer between the fluorophores and the metal surface. An extrapolation of the experimental data suggests that the very strong fluorescence quenching *extends over several tens of nanometers*, well-beyond usual distances below 10 nm. This intriguing phenomenon offers a new possibility for the detection of fluorescent markers at a much more expanded spatial scale than that exploited in current sensing arrays.

Free standing nanomembranes with robust fluorescence. To test whether the fluorescent properties of these LbL films can be retained in the free-suspended state which is important for prospective sensing applications, we transferred the fluorescent 9*G 9* LbL film with encapsulated gold nanoparticles across a 150 μm opening (Fig. 7a).^[52–54] These freely suspended LbL films were mechanically robust, sustained large deformations, and retained high fluorescence contrast. The fluorescent properties of the LbL film were tested by collecting the fluorescence spectra while mechanically deforming film by applying air pressure (bulging test).^[29,55–57]

The fluorescence spectra obtained from the nanomembrane under increasing pressure is depicted in Fig. 7b with the inset showing the peak position for different pressures. Apparently, except for minor changes in the intensity due to minor photobleaching and changing film position (several micron deflection) during deformation, a very stable fluorescence signature is preserved for widely deformed freely suspended LbL films. This robust optical signature of fluorescent LbL films under significant mechanical deformation can be important for prospective chemical sensing applications in which the fluorescence response can be monitored in the course of interaction with the active environment. The micropatterned, freely-suspended LbL membranes demonstrated in the current study can be critical for a wide variety of experiments involving fluorescent labels such as diffusion kinetics, transport, binding, and trace analysis over large distances. The reported LbL architecture with partially suppressed photobleaching, efficient fluorescent

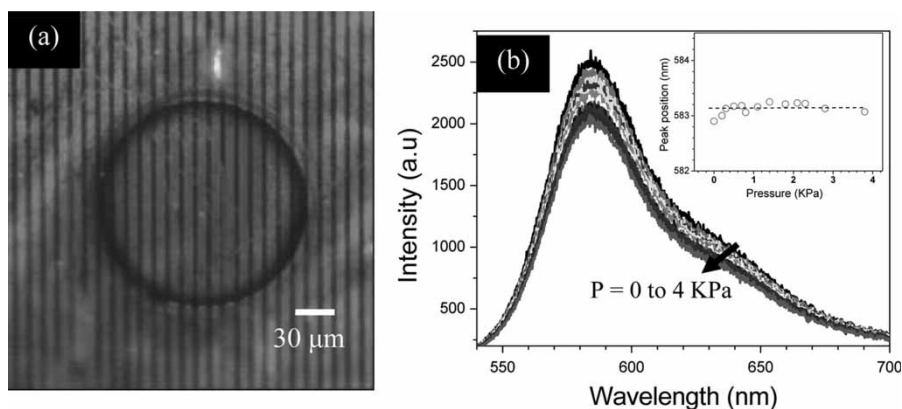


Figure 7. (a) Fluorescence image of the 9*G 9* LbL film freely suspended over 150 μm opening. (b) Fluorescence spectra of this LbL films under hydrostatic pressures ranging from 0 to 4 K Pa (inset displays the peak position variation vs. pressure).

quenching extending over distances of 20–50 nm, and stable fluorescent signature can be applied to layered spherical microparticles to produce highly stable and long-range fluorescent beads potentially replacing the conventional fluorescent tags which suffer from fast bleaching and short-range quenching phenomenon.

Acknowledgments

The authors thank Prof. Y. Lvov for his suggestions in labeling the polyelectrolytes. The authors thank H. Ko for invaluable help with micropatterning and M.E. McConney for useful discussions. This work was supported by the AFOSR, FA9550-05-1-0209 and NSF-CTS-0506832 Grants.

References

1. Hemmila, I.A. *Applications of Fluorescence in Immunoassays*; John Wiley: New York, 1991.
2. Pearson, J.E.; Gill, A.; Vadgama, P. Analytical aspects of biosensors. *Ann. Clin. Biochem.* **2000**, *37*, 119.
3. Dubertret, B.; Calame, M.; Libchaber, A.J. Single-mismatch detection using gold-quenched fluorescent oligonucleotides. *Nat. Biotechnol.* **2001**, *19*, 365.
4. Maxwell, D.J.; Taylor, J.R.; Nie, S. Self-assembled nanoparticle probes for recognition and detection of biomolecules. *J. Am. Chem. Soc.* **2002**, *124*, 9606.
5. Aslam, K.; Perez-Luna, V.H. Quenched emission of fluorescence by ligand functionalized gold nanoparticles. *J. Fluoresc.* **2004**, *14*, 401.
6. Gosling, J.P. A decade of development in immunoassay methodology. *Clin. Chem.* **1980**, *36*, 1408.
7. Matveeva, E.; Gryczynski, Z.; Malicka, J.; Gryczynski, I.; Lakowicz, J.R. Metal-enhanced fluorescence immunoassays using total internal reflection and silver island-coated surfaces. *Anal. Biochem.* **2004**, *334*, 303.
8. Zhuang, X.; Ha, T.; Kim, H.D.; Centner, T.; Labeit, S.; Chu, S. Fluorescence quenching: A tool for single-molecule protein-folding study. *P. Natl. Acad. Sci.* **2000**, *97*, 14241.
9. Miyawaki, A.; Tsien, R.Y. Monitoring protein conformations and interactions by fluorescence resonance energy transfer between mutants of green fluorescent protein. *Method. Enzymol.* **2000**, *327*, 472.

10. Chance, R.R.; Prock, A.; Silbey, R. Molecular fluorescence and energy transfer near interfaces. *Adv. Chem. Phys.* **1978**, *37*, 1.
11. Förster, T. Zwischenmolekulare Energiewanderung und Fluoreszenz. *Ann. Phys.* **1948**, *2*, 55.
12. Gerston, J.; Nitzan, A. Spectroscopic properties of molecules interacting with small dielectric particles. *J. Chem. Phys.* **1981**, *75*, 1139.
13. Dulkeith, E.; Ringler, M.; Klar, T.A.; Fledmann, J.; Munoz Javier, A.; Parak, W.J. Gold nanoparticles quench fluorescence by phase induced radiative rate suppression. *NanoLett.* **2005**, *5*, 585.
14. Dulkeith, E.; Morteani, A.C.; Niedereichholz, T.; Klar, T.A.; Feldmann, J.; Levi, S.A.; van Veggel, F.C.J.M.; Reinhoudt, D.N.; Moller, M.; Gittins, D.I. Fluorescence quenching of dye molecules near gold nanoparticles: radiative and nonradiative effects. *Phys. Rev. Lett.* **2002**, *89*, 203002.
15. Lindquist, G.A. A flash photolysis study of fluorescein. *Ark. Kem.* **1960**, *16*, 79.
16. Nehls, S.; Snapp, E.L.; Cole, N.B.; Zaal, K.J.M.; Kenworthy, A.K.; Roberts, T.H.; Ellenberg, J.; Presley, J.F.; Siggia, E.; Lippincott-Schwartz, J. Dynamics and retention of misfolded proteins in native ER membranes. *Nat. Cell Bio.* **2000**, *2*, 288.
17. Yguerabide, J.; Schmidt, J.A.; Yguerabide, E.E. Lateral mobility in membranes as detected by fluorescence recovery after photobleaching. *Biophys. J.* **1982**, *40*, 69.
18. Berrios, M.; Conlon, K.A.; Colflesh, D.E. Antifading agents for confocal fluorescence microscopy. *Methods Enzymol.* **1999**, *307*, 55.
19. Bencic-Nagale, S.; Walt, D.R. Extending the longevity of fluorescence-based sensor arrays using adaptive exposure. *Anal. Chem.* **2005**, *77*, 6155.
20. McClure, D.S. *Electronic Spectra of Molecules and Ions in Crystals*; Academic Press: New York, 1959.
21. Jablonski, J. Self-depolarization and decay of photoluminescence of solutions. *Acta Phys. Pol.* **1955**, *XIV*, 295.
22. Han, K.; Lu, X.; Xu, J.; Zhou, G.; Ma, S.; Wang, W.; Cai, Z.; Zhou, J. Spectral and dynamic studies on molecular aggregation in hemicyanine Langmuir–Blodgett films. *J. Phys. D: Appl. Phys.* **1997**, *30*, 2923.
23. Hua, F.; Lvov, Y.; Cui, T. A lithographic approach of spatial separation for multiple types of layer-by-layer self-assembled nanoparticles. *Thin Solid Films* **2004**, *449*, 222.
24. Lvov, Y.; Mohwald, H. *Protein Architecture Interfacing Molecular Assemblies and Immobilization Biotechnology*; Marcel Dekker Inc: New York, 2000.
25. Decher, G. Fuzzy nanoassemblies: Toward layered polymeric multicomposites. *Science* **1997**, *277*, 1232.
26. Decher, G.; Schlenoff, J.B. Eds. *Multilayer thin films*; Wiley-VCH: Weinheim, Germany, 2003.
27. Hammond, P.T. Form and function in multilayer assembly: New applications at the nanoscale. *Adv. Mater.* **2004**, *16*, 1271.
28. Schönhoff, M. Layered polyelectrolyte complexes: Physics of formation and molecular properties. *J. Phys.: Condens. Mat.* **2003**, *15*, R1781.
29. Jiang, C.; Markutsya, S.; Pikus, Y.; Tsukruk, V.V. Freely suspended nanocomposite membranes as highly sensitive sensors. *Nat. Mater.* **2004**, *3*, 721.
30. Ko, H.; Jiang, C.; Shulha, H.; Tsukruk, V.V. Carbon nanotube arrays encapsulated into freely suspended flexible films. *Chem. Mater.* **2005**, *17*, 2490.
31. Jiang, C.; Rybak, B.M.; Markutsya, S.; Kladitis, P.E.; Tsukruk, V.V. Self-recovery of stressed nanomembranes. *Appl. Phys. Lett.* **2005**, *86*, 121912.
32. Kotov, N.A.; Dekany, I.; Fendler, J.H. Ultrathin graphite oxide-polyelectrolyte composites prepared by self-assembly: transition between conductive and non-conductive states. *Adv. Mater.* **1996**, *8*, 637.
33. Zheng, H.P.; Lee, I.; Rubner, M.F.; Hammond, P.T. Two component particle arrays on patterned polyelectrolyte multilayer templates. *Adv. Mater.* **2002**, *14*, 569.
34. Ko, H.; Jiang, C.; Tsukruk, V.V. Encapsulating nanoparticle arrays into layer-by-layer multilayers by capillary transfer lithography. *Chem. Mater.* **2005**, *17*, 5489.

35. Ibarz, G.; Dähne, L.; Donath, E.; Möhwald, H. Smart micro- and nanocontainers for storage, transport, and release. *Adv. Mater.* **2001**, *13*, 1324.
36. Grabar, K.C.; Freeman, R.G.; Hommer, M.B.; Natan, M.J. Preparation and characterization of Au colloid monolayers. *Anal. Chem.* **1995**, *67*, 735.
37. Jiang, C.; Markutsya, S.; Tsukruk, V.V. Collective and individual plasmon resonances in nanoparticle films obtained by spin-assisted layer-by-layer assembly. *Langmuir* **2004**, *20*, 882.
38. Cho, J.; Char, K.; Hong, J.-D.; Lee, K.-B. Fabrication of highly ordered multilayer films using a spin self-assembly method. *Adv. Mater.* **2001**, *13*, 1076.
39. Tsukruk, V.V. Scanning probe microscopy of polymer surfaces. *Rubber Chem. Tech.* **1997**, *70*, 430.
40. Tsukruk, V.V.; Reneker, D.H. Scanning probe microscopy of polymeric and organic molecular films: from self-assembled monolayers to composite multilayers. *Polymer* **1995**, *36*, 1791.
41. Ko, H.; Pikus, Y.; Jiang, C.; Jauss, A.; Hollricher, O.; Tsukruk, V.V. High-resolution Raman microscopy of curled carbon nanotubes. *Appl. Phys. Lett.* **2004**, *85*, 2598.
42. Brismar, H.; Trepte, O.; Ulfhake, B. J. Spectra and fluorescence lifetimes of lissamine rhodamine, tetramethylrhodamine isothiocyanate, Texas Red, and cyanine 3.18 fluorophores: influences of some environmental factors recorded with a confocal laser scanning microscope. *Histochem. Cytochem.* **1995**, *43*, 699.
43. Young, M.C.J.; Jones, R.; Tredgold, R.H.; Lu, W.X.; Ali-Adib, Z.; Hodge, P.; Abbasi, F. Optical and structural characterization of Langmuir-Blodgett multilayers of non-polymeric and polymeric hemicyanines. *Thin Solid Films* **1989**, *182*, 319.
44. Ulman, A. An introduction to Ultrathin organic films From Langmuir-Blodgett to Self assembly. Academic Press, Inc: San Diego, 1991.
45. Tong-Sheng, C.; Shao-Qun, Z.; Wei, Z.; Qing-Ming, L. A quantitative theory model of a photobleaching mechanism. *Chinese Phys. Lett.* **2003**, *20*, 1940.
46. Bene, L. Nanoparticle energy transfer on the cell surface. *J. Molec. Recog.* **2005**, *18*, 236.
47. Lakowicz, J.R. Principles of Fluorescence Spectroscopy Kluwer. Academic/Plenum Publisher: New York, 1999.
48. Alivisatos, A.P.; Waldeck, D.H.; Harris, C.B. Nonclassical behavior of energy transfer from molecules to metal surfaces: Biacetyl(${}^3n\pi^*$)/Ag(111). *J. Chem. Phys.* **1985**, *82*, 541.
49. Yun, C.S.; Javier, A.; Jennings, T.; Fisher, M.; Hira, S.; Peterson, S.; Hopkins, B.; Reich, N.O.; Strouse, G.F. Nanometal surface energy transfer in optical rulers, breaking the FRET barrier. *J. Am. Chem. Soc.* **2005**, *127*, 3115.
50. Kuhn, H.J. Classical aspects of energy transfer in molecular systems. *J. Chem. Phys.* **1970**, *53*, 101.
51. Schneider, G.; Decher, G.; Nerambourg, N.; Praho, R.; Werts, M.H.V.; Blanchard-Desce, M. Distance-dependent fluorescence quenching on gold nanoparticles ensheathed with layer-by-layer assembled polyelectrolytes. *NanoLett.* **2006**, *6*, 530.
52. Jiang, C.; McConney, M.E.; Singamaneni, S.; Merrick, E.; Chen, Y.; Zhao, J.; Zhang, L.; Tsukruk, V.V. Thermo-optical arrays of flexible nanoscale nanomembranes freely suspended over microfabricated cavities as IR microimagers. *Chem. Mater.* **2006**, *18*, 2632.
53. Jiang, C.; Tsukruk, V.V. Free standing nanostructures via layer-by-layer assembly. *Adv. Mater.* **2006**, *18*, 829.
54. Jiang, C.; Markutsya, S.; Tsukruk, V.V. Compliant, robust, and truly nanoscale free-standing multilayer films fabricated using spin-assisted layer-by-layer assembly. *Adv. Mater.* **2004**, *16*, 157.
55. Markutsya, S.; Jiang, C.; Pikus, Y.; Tsukruk, V.V. Freely suspended layer-by-layer nanomembranes: testing micromechanical properties. *Adv. Funct. Mater.* **2005**, *15*, 771.
56. Jiang, C.; Lio, W.Y.; Tsukruk, V.V. Surface enhanced Raman scattering monitoring of chain alignment in freely suspended nanomembranes. *Phys. Rev. Lett.* **2005**, *95*, 115503.
57. Jiang, C.; Markutsya, S.; Shulha, H.; Tsukruk, V.V. Freely suspended gold nanoparticles arrays. *Adv. Mater.* **2005**, *17*, 1669.